*International Journal of Minerals, Metallurgy and Materials*
*Volume 17, Number 5, October 2010, Page 579*
**DOI: 10.1007/s12613-010-0360-2**

# Hydrogen induced cracking of X80 pipeline steel

*Chao-fang Dong, Kui Xiao, Zhi-yong Liu, Wen-jing Yang, and Xiao-gang Li*

Corrosion and Protection Center, University of Science and Technology Beijing, Beijing 100083, China
(Received: 15 November 2009; revised: 20 December 2009; accepted: 25 December 2009)

**Abstract:** The hydrogen-induced cracking (HIC) behavior of X80 pipeline steel was studied by means of electrochemical charging, hydrogen permeation tests, tension test, and scanning electron microscopy (SEM). The experimental results indicate that the increase of charging time and charging current density or the decrease of the solution pH value leads to an increase of the hydrogen content in X80 steel, which plays a key role in the initiation and propagation of HIC. It is found that the majority of macro-inclusions within the as-used X80 steel do not constitute a direct threat to HIC except aluminum oxides, which directly or indirectly lead to HIC. The hydrogen trap density at room temperature is estimated to be pretty high, and this is an essential reason why the steel is sensitive to HIC. After hydrogen charging, the elongation loss rate and area reduction of X80 steel decline obviously, taking a noticeable sign of hydrogen-induced plasticity damages. It is demonstrated that the losses of these plastic parameters have a linear relation to the fracture size due to hydrogen.

**Keywords:** pipeline steel; hydrogen induced cracking; electrochemical charging; fracture

[*This work was financially supported by the National Natural Science Foundation of China (No.50401016).*]

## 1. Introduction

With the development of the petroleum industry, the oil-gas pipeline is developed rapidly in terms of safety, economy and efficiency. With the increase of gas pressure, high strength pipeline steels are being widely used in various projects [1]. X80 pipeline steel, as a high strength pipeline steel, is becoming one of the most widely applied pipe materials because of its high strength and toughness which not only save lots of steel, but also have a better performance [2-3]. However, hydrogen induced cracking (HIC) has been acknowledged as one of the predominant failures in pipeline steel in humid environments with $H_2S$ and other sour materials, which causes the heavy leakage of oil as well as the serious economic loss and casualties [4-5].

Up to now, a lot of work has been done to investigate the property of X80 pipeline steel. Hardie *et al.* [6] compared the susceptibility of three kinds of API pipeline steels (X60, X80, and X100 grades) to hydrogen embitterment, showing that the increase of strength level tends to decrease the resistance of steels to HIC. Sang *et al.* [7] studied the relationship between the microstructure and Charpy impact properties of X70 and X80 pipeline steels. Shterenlikht *et al.* [8] reported the capacity of the anti-ductile crack growth of X80 pipeline steels. Kong *et al.* [9] reported the effect of Mo on the microstructure and mechanical properties of X80 pipeline steel. However, the specifics for HIC of X80 pipeline steel, and additionally the impact of inclusions on HIC and the mechanical properties of the steel are still unknown. In view of this, it is extremely necessary to work out the details of hydrogen-induced damages and how these failures deteriorate the properties of X80 pipeline.

Hydrogen induced cracking in X80 pipeline steel under various electrochemical hydrogen-charging conditions as well as the influence of inclusions and microstructure on the origin of HIC were investigated in this work. The detailed characteristics of hydrogen in the metal matrix, such as the diffusivity of hydrogen ($D_{eff}$) and the hydrogen content at

Corresponding author: Chao-fang Dong E-mail: cfdong@ustb.edu.cn
© University of Science and Technology Beijing and Springer-Verlag Berlin Heidelberg 2010

room temperature, were measured to attempt to explore the critical condition of the occurrence of HIC in X80 steel. In combination, the mechanical performance after electrochemical hydrogen charging was separately studied to understand the extent of HIC on the mechanical properties of X80 steel under different hydrogen contents.

## 2. Experimental

### 2.1. Material

The samples of X80 pipeline steel were cut from a commercial steel plate with the chemical composition (wt%) of 0.089 C, 0.16 Si, 1.63 Mn, 0.0025 S, 0.011 P, 0.12 Cu, 0.058 Nb, 0.017 Ti, 0.43 Mo, and the balance Fe. The microstructure of the as-received X80 pipeline steel is shown in Fig. 1, which exhibits that there are predominantly bainites and some ferrites.

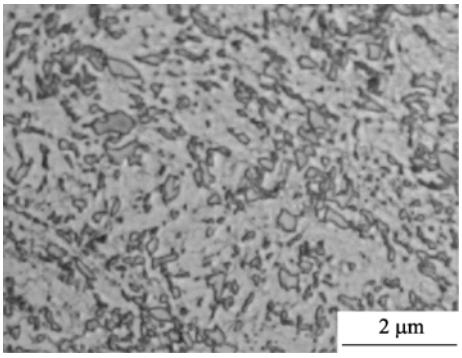


**Fig. 1. Microstructure of the X80 pipeline steel.**

### 2.2. Electrochemical hydrogen charging

For the electrochemical charging test at room temperature, the 2-mm thick specimens were prepared with the charging surface polished to a mirror finish. The $H_2SO_4$ solutions of different concentrations (such as 0.05, 0.1, and 0.5 mol/L) with 250 mg/L arsenic trioxide ($As_2O_3$) as the hydrogen evolution poison were used as the hydrogen charging solutions, which are widely used as a kind of simulating condition in laboratories involving hydrogen revolution environments, such as $H_2S$ condition [10-12]. The charging current densities were 20, 50, and 100 mA/cm$^2$, and the charging times were 1, 3, 5, and 8 h, respectively. The hydrogen-charged specimens were immediately immersed in liquid paraffin to measure the release flux of hydrogen using a scaled cuvette as the hydrogen gas collecting container. After charging with a current density of 20 mA/cm$^2$, the hydrogen-induced cracking size was measured through scanning electron microscopy (SEM).

### 2.3. Hydrogen permeation test

For the hydrogen permeation test, the specimens were prepared with a surface area of 1.76 cm$^2$ and a thickness of 0.56 mm. The samples were electrolytically coated with nickel on both sides prior to the test to get the significant hydrogen permeation current density.

The hydrogen permeation test was performed using a double cell. The cathodic side of the cell contained a solution of 0.5 mol/L $H_2SO_4$ with 250 mg/L $As_2O_3$ added as the hydrogen evolution poison. The hydrogen ingress into the specimen was facilitated by maintaining a constant cathodic current of 10 mA/cm$^2$. The anodic side, *i.e.*, the hydrogen exit side, contained 0.1 mol/L NaOH solution and was potentiostatically polarized at a constant potential of 300 mV *vs.* a saturated calomel electrode (SCE). Before the hydrogen permeation test, the anodic side of the double cell was piped into nitrogen to remove the dissolved oxygen in the solution.

### 2.4. Tension test

The flat test bars of X80 pipeline steel used here were prepared along the rolling direction. Then, the specimens were ground longitudinally with 2000-grade emery paper, masked with the exception of the gauge length, and then degreased before charging. Hydrogen charging was carried out in 0.5 mol/L $H_2SO_4$ solution with 250 mg/L $As_2O_3$ as the hydrogen evolution poison under a cathodic current of 20 mA/cm$^2$ for 1, 5, and 8 h, correspondingly. The specimens were kept in liquid nitrogen after hydrogen charging before being brought out and fixed in a tension machine to measure the mechanical property. The sample setting time and measure time in the air were less than 2 min. The rate of the tension test was 0.2 mm/s. The effect of hydrogen on ductility was assessed by comparing the elongation and the reduction in area before and after charging.

## 3. Results and discussion

### 3.1. Hydrogen-induced cracking property in X80 steel

After hydrogen charging, the X80 pipeline steel sample was immersed in liquid paraffin at once to measure the hydrogen release content. Fig. 2 shows that the hydrogen release content of X80 steel increases as the charging current intensified, the charging solution concentrated (Figs. 2(a)-(b)), as well as the charging time elongated (Fig. 2(b)). It reveals that the hydrogen content of X80 steel increases under the hydrogen revolution condition, which leads to the cracking failure if the hydrogen content is high enough in some local positions.

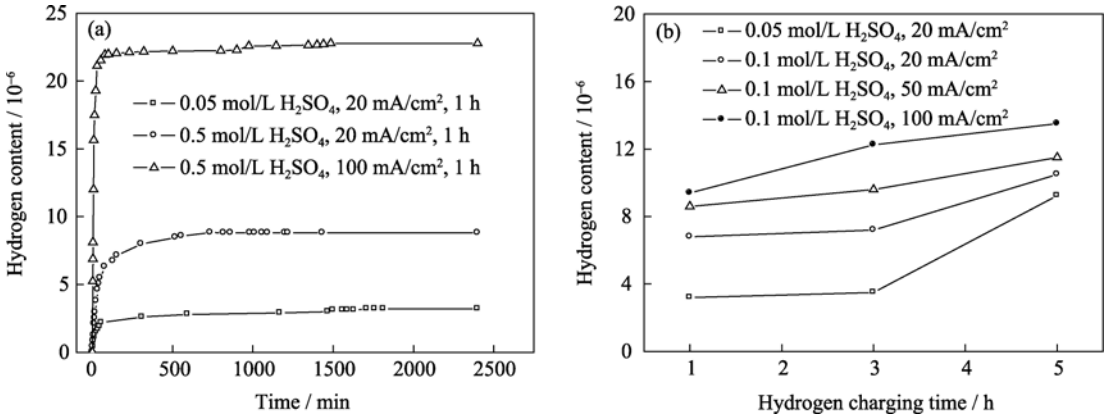


**Fig. 2. Amount of hydrogen release from the X80 pipeline steel specimens: (a) charging with solutions of different concentrations and at different current densities for 1 h; (b) charging under various conditions.**

Usually, hydrogen-induced blisters are considered as a kind of hydrogen-induced cracks which just take place in a shallow position. Thus, the growing process of hydrogen blisters may reflect the information of HIC growing. Fig. 3 shows the process of hydrogen-induced blisters in the initiation and growth periods along with the charging time increasing. It can be seen that after 1-h charging, some tiny scale blisters can be found on the metal surface in Fig. 3(a), and these blisters extend rapidly as the charging time increases as shown in Figs. 3(b)-(d). It indicates that hydrogen-induced damages, such as blisters and cracks, may initiate and grow soon in an intensive hydrogen revolution condition, *i.e.*, X80 steel cannot be immune to hydrogen-induced damages.

The sizes of hydrogen-induced cracks vary according to the charging condition. As the time increases, the solution pH value gets lower, or the current density becomes higher, the sizes of cracks tend to get bigger, and the density of cracks has a tendency to multiply. In this work, the statistics of crack size under the charging current density of 20 $mA/cm^2$ in the solution of 0.5 mol/L $H_2SO_4$ with 250 mg/L $As_2O_3$ as the hydrogen evolution poison is shown in Fig. 4. Both the crack length and width extend quickly within the charging time of 3 h, and then grow at a slower rate as the

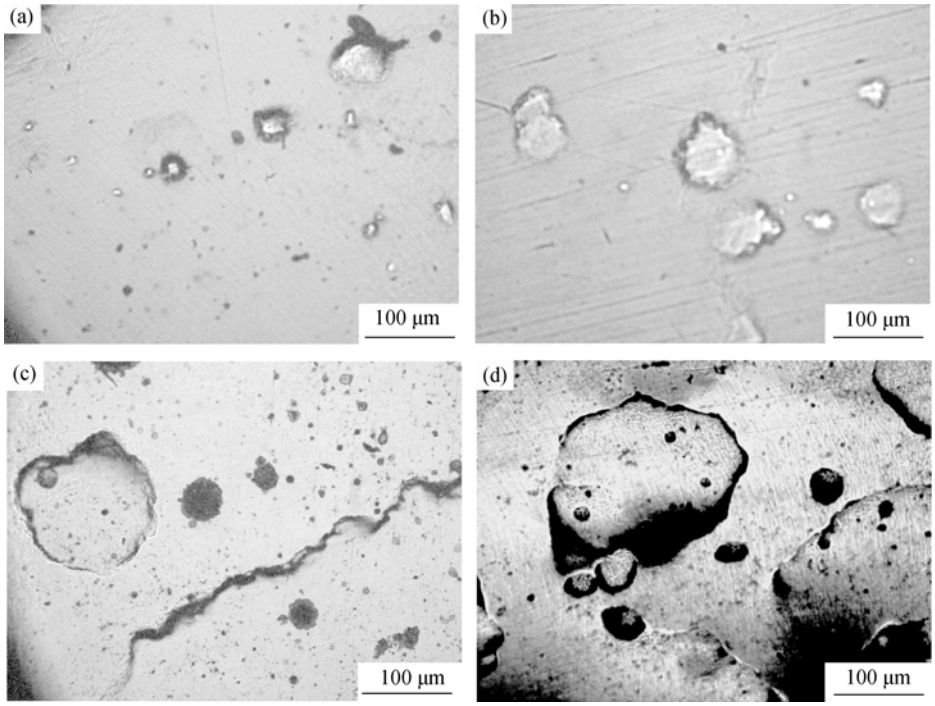


**Fig. 3. Morphologies of hydrogen-induced blisters in the X80 steel sample after charging with the current density of 50 $mA/cm^2$ in the solution of 0.5 mol/L $H_2SO_4$ for different charging time: (a) 1 h; (b) 3 h; (c) 5 h; (d) 8 h.**

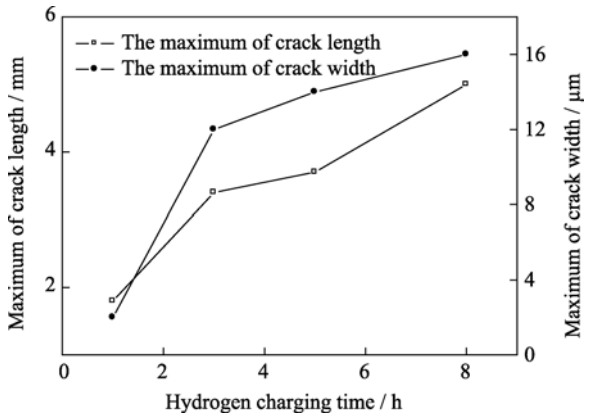


**Fig. 4. Statistics of crack size obtained under the charging current density of 20 mA/cm2 in the solution of 0.5 mol/L $H_2SO_4$ with 250 mg/L $As_2O_3$ as the hydrogen evolution poison.**

charging time increases, which reveals that HIC initiates and grows fast in the early stage under a constant charging condition, and then propagates at a relatively slower rate.

Being of great importance for hydrogen damage and hydrogen induced cracking, the solute atoms, cavities, dislocations, grain boundaries, and other inclusions of steel are all hydrogen traps. Fig. 1 shows that the grain of X80 pipeline steel is very fine with an average diameter less than 9 μm. Thus, the density of grain boundaries is relatively high. There are various types of inclusions in the X80 steel identified as follows: mainly aluminum oxides with slight oxides and nitrides of Ti and Ni, and slight amounts of oxides and carbides of Ca, Mg, and Si. Because of 0.0025wt% S and 1.63wt% Mn in the X80 pipeline steel, a small chance for MnS is observed by SEM. The type of inclusions is consistent with Ref. [13].

In the as-used X80 pipeline steel, there are various types of inclusions and the most familiar species is aluminum oxides in the shape of triangle, polygon, or circle. Sometimes, it becomes bright because of the discharge. In the SEM observations in Fig. 5, the mixture of various inclusions can be seen. They show that the sizes of inclusions are generally 2 μm, and the bigger ones are ranging from 5 to 10 μm. Most of the inclusion sizes are smaller than the grain diameter. Thus, it is really difficult to determine whether the inclusions locate in intergranular or transgranular positions.

There are a large amount of aluminum oxide inclusions in the cracks as well as in the X80 steel bulk matrix as shown in Fig. 5. Though there are usually some other kinds of inclusions mixed with aluminum oxides, such as oxides of Si, Ca, and Mg, these inclusions are less sensitive to promote the initiation of HIC or stress corrosion cracking induced by HIC in a hydrogen revolution environment [14].

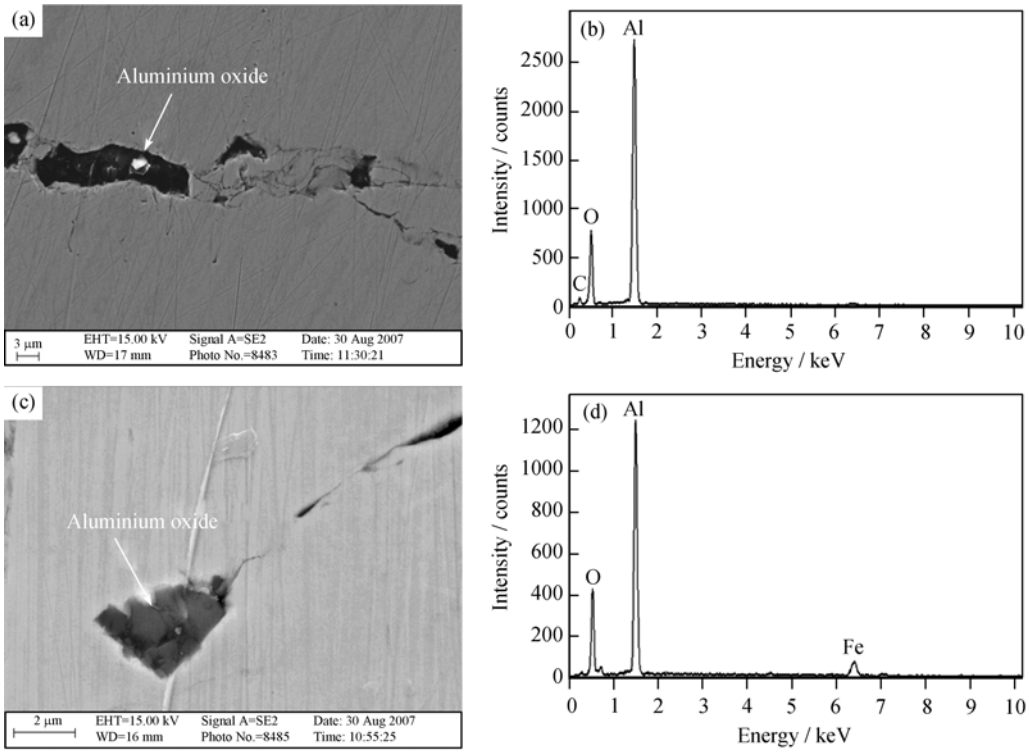


**Fig. 5. Inclusions in cracks of X80 steel: (a) microstructure of aluminum oxides; (b) EDX spectrum of the aluminium oxides; (c) microstructure of aluminum oxides; (d) EDX spectrum of the aluminium oxides.**

It also has been mentioned [15] that HIC germinates from the inclusion cluster of MnS or $Al_2O_3$. Therefore, aluminum oxides are found as the major inclusions associated with HIC in Fig. 5.

On the interface between nonmetals and the basal body, cavities appear due to different thermal expansion coefficients, and it is much easier for hydrogen to conglomerate in these cavities, then the emergence of cracks leads to cusp stress concentration. In this test, cracks caused by MnS were not observed, and the hydrogen-induced cracks associated with a large quantity of aluminum oxides were surveyed, which generally conforms to Ref. [15].

X80 pipeline steel is a type of high strength low alloy steel, and some microalloy elements, such as Ti and Nb, are added mainly to form titanium nitrides to refine grains. Additionally, these microalloy elements can prevent the formation of Widmanstätten and coarse grained bainites. According to Ref. [16], there is no obvious relation between hydrogen-induced fractures and macro inclusions in super high strength steel. Also, MnS, TiN, and silicate are not the sources of HIC. Combining the experimental research, it is reasonable to believe that the majority of macro-inclusions in the as-received X80 steel do not constitute a direct threat to hydrogen induced cracking except aluminum oxides in the electrochemical hydrogen charging conditions, which directly or indirectly lead to the majority of HIC in the experiment.

In the test, cracks of about 0.4-1.6 mm deep in the surface can be found, and the macro hydrogen-induced cracks are about 16 μm in width as shown in Fig. 4. On account of fine grains of X80 pipeline steel and the macro HIC of 2-16 μm in width, it is really difficult to determine whether the expansion of macro cracks is intergranular or transgranular. As for much narrower hydrogen-induced cracks, they are mostly transgranular as shown in Fig. 6.

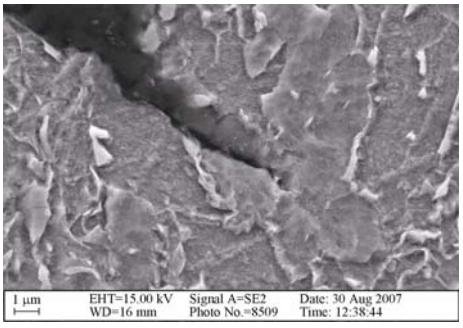


**Fig. 6. Transgranular cracks in X80 pipeline steel.**

### 3.2. Hydrogen diffusion in X80 pipeline steel

Fig. 7 shows the hydrogen permeation curve of the as-received X80 steel. The hydrogen flux through the specimen was measured by saturated anode current density ($I_\infty$), and converted into the hydrogen permeation flux according to Eq. (1) [17]:

$$J_\infty = \frac{I_\infty}{FA} \tag{1}$$

where $A$ is the area of the specimen where diffusion appears, $F$ the Faraday constant, and $J_\infty$ the hydrogen permeation flux.

The effective hydrogen diffusivity ($D_{\text{eff}}$) can be calculated by Eq. (2) [18].

$$D_{\text{eff}} = \frac{d^2}{6t_{\text{L}}} \tag{2}$$

where $d$ is the thickness of the specimen and $t_{\text{L}}$ is the time lag when $I/I_\infty$ equals to 0.63.

The hydrogen content at the cathodic side ($C_0$) can be estimated by Eq. 3 [19].

$$C_0 = \frac{J_\infty \cdot d}{D_{\text{eff}}} \tag{3}$$

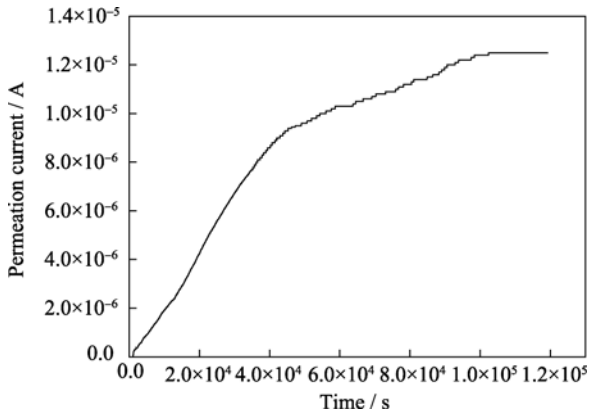


**Fig. 7. Hydrogen permeation curve of the X80 steel.**

As known from the hydrogen permeation curve in Fig. 7, $I_\infty$=12.5 μA and $t_{\text{L}}$=97560 s, as well as $A$=1.76 cm$^2$ and $d$=0.056 cm, these values are substituted into Eqs. (1)-(3).

$$J_\infty = \frac{I_\infty}{FA} = \frac{12.5\times10^{-6}}{96500\times1.767} = 7.36\times10^{-11}\ \text{mol}\cdot\text{cm}^{-2}\cdot\text{s}^{-1} \tag{4}$$

$$D_{\text{eff}} = \frac{d^2}{6t_{\text{L}}} = \frac{0.0557^2}{6\times97560} = 5.32\times10^{-9}\ \text{cm}^2\cdot\text{s}^{-1} \tag{5}$$

$$C_0 = \frac{J_\infty \cdot d}{D_{\text{eff}}} = \frac{7.36\times10^{-11}\times0.0557}{5.32\times10^{-9}} = 7.71\times10^{-4}\ \text{mol}\cdot\text{cm}^{-3} \quad (6)$$

The hydrogen trap density can be estimated as

$$\ln\left(\frac{D_L}{D_{\text{eff}}}-1\right) = \ln\frac{N_T}{N_L} + \frac{E_b}{R}\cdot\frac{1}{T} \quad (7)$$

$$N_T = N_L\cdot\left(\frac{D_L}{D_{\text{eff}}}-1\right)\cdot\exp\left(-\frac{E_b}{RT}\right) \quad (8)$$

where $N_T$ is the number of hydrogen trapping sites per unit volume, $cm^{-3}$; $D_L$ the lattice diffusion coefficient, $cm^{-3}\cdot s^{-1}$; $N_L$ the density of the interstitial sites, $cm^{-3}$; $E_b$ the trap binding energy, eV; $R$ the molar gas constant, 8.3145 $J\cdot mol^{-1}\cdot K^{-1}$; and $T$ the temperature, 298 K.

In the test, because of the absence of $D_L$, $E_b$, and $N_L$, the diffusion coefficient of α-Fe is replaced [16], in other words, $D_L$=1.28×10$^{-4}$ $cm^{-3}\cdot s^{-1}$, $E_b$=0.3 eV, $N_L$=7.52×10$^{22}$ $cm^{-3}$, and the values of $D_{\text{eff}}$ are calculated from the Eq. (5), and these values are substituted into Eq. (8):

$$N_T = 7.52\times10^{22}\times\left(\frac{1.28\times10^{-4}}{5.32\times10^{-9}}-1\right)\times\exp\left(-\frac{0.3}{8.3145\times300}\right) = 1.609\times10^{27}\ \text{cm}^{-3} \quad (9)$$

According to Eq. (8), the density of hydrogen trap positions in X80 steel is tremendously high, which indicates that hydrogen is easy to be trapped in this metal resulting in the occurrence of cracks.

### 3.3. Effect of hydrogen on the strength of X80 pipeline steel

The stress-displacement curves of the specimen after electrochemical hydrogen charging are shown in Fig. 8. It indicates that, in the solution of 0.5 mol/L $H_2SO_4$ with a constant current density of 20 $mA/cm^2$, the tensile strength begins to slightly decline in limited scale as the charging time becomes longer. It is usually believed that hydrogen has little or trivial influence on the tensile strength of the specimen, but under the condition of electrochemical hydrogen charging in this test, nonreciprocal hydrogen-induced damages appear on the surface and inside part, including both micro cracks and macro cracks visible to the naked eye, so the tensile strength declines.

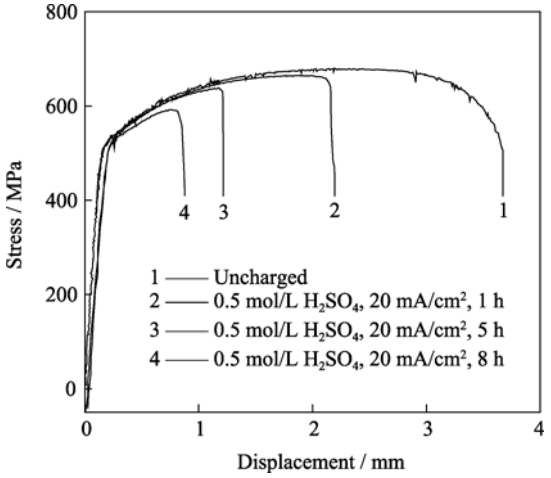


**Fig. 8. Stress-displacement curves of the X80 steel under different charging conditions.**

Percentage elongation ($\delta$) and reduction in area ($\psi$) are the usual indexes of plasticity. Additionally, the relative plasticity damages (the elongation loss rates ($I_\delta$) and area reduction ($I_\psi$)) are used to evaluate the sensitivity of hydrogen embrittlement:

$$\begin{cases} I_\delta = (\delta_0 - \delta_H)/\delta_0\times100\% \\ I_\psi = (\psi_0 - \psi_H)/\psi_0\times100\% \end{cases} \quad (10)$$

where $\delta_0$ and $\delta_H$ are the elongation of the steel before and after hydrogen charging, respectively; and $\psi_0$ and $\psi_H$ are the reduction in area before and after hydrogen charging, respectively.

Fig. 9 indicates the changes of $\delta$ and $\psi$ according to charging time. When the charging time becomes longer, the content of hydrogen tends to increase, and the plasticity of the as-used X80 steel tends to decline greatly. The change of relative plasticity damages ($I_\delta$ and $I_\psi$) are listed in Table 1,

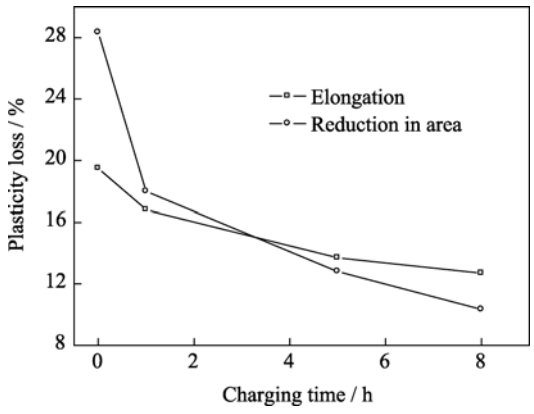


**Fig. 9. Plasticity loss of the X80 steel.**

**Table 1. Relative plasticity damages of X80 pipeline steel after hydrogen charging**

| Charging time / h | $I_\delta$ / % | $I_\psi$ / % |
|---|---|---|
| 1 | 13.85 | 36.54 |
| 5 | 29.74 | 54.81 |
| 8 | 34.87 | 63.52 |

both of which increase with the increase of charging time to confirm the tendency of the effect of hydrogen charging on plastic shift.

The fracture morphologies of the specimen are shown in Fig. 10. When the specimen without hydrogen charging is subjected to the tensile test in air, the fracture shows a typical shape of dimple morphology (Fig. 10(a)). As hydrogen charging is applied and the charging time becomes longer, though the fracture still generally exhibits a dimple morphology, the embrittlement susceptibility of the material rises, the scale of dimples is enhanced after 3-h charging with brittle morphology in some local areas, as shown in Figs. 10(b)-(d).

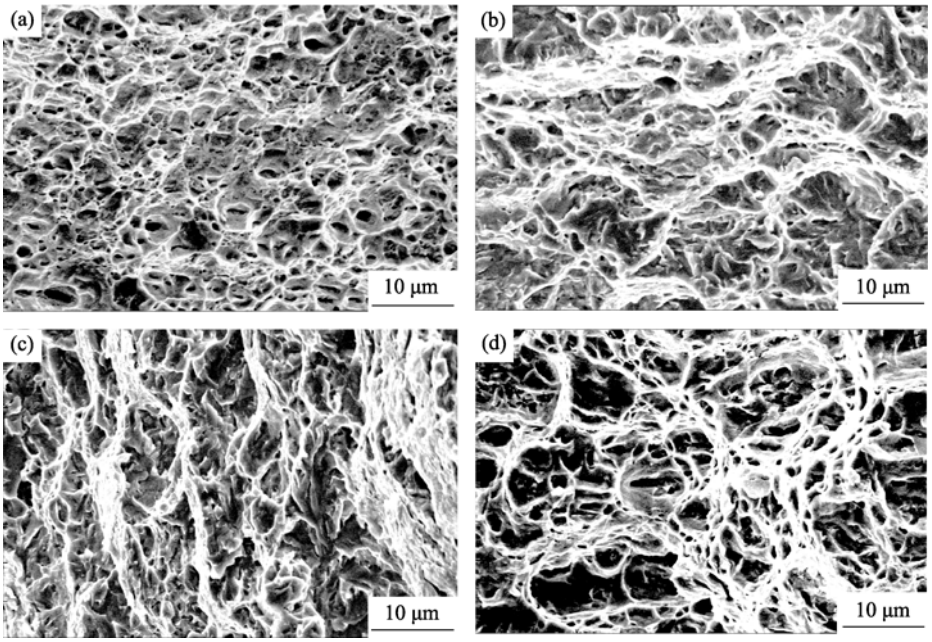


**Fig. 10. Tension fracture surface of the X80 pipeline steel before (a) and after hydrogen charging: (b) 0.5 mol/L $H_2SO_4$, 20 mA/cm$^2$, 1 h; (c) 0.5 mol/L $H_2SO_4$, 20 mA/cm$^2$, 3 h; (d) 0.5 mol/L $H_2SO_4$, 20 mA/cm$^2$, 5 h.**

According to the results in Fig. 2, the hydrogen content in X80 steel increases with extending the charging time, concentrating the charging solution, or increasing the charging current density. HIC appears and grows up when the hydrogen content increases (shown in Fig. 3), as well as when the charging time increases (shown in Fig. 4). These lead to the damage of the mechanical properties of X80 steel, *i.e.*, hydrogen failures in the bulk body of the X80 steel sample accelerate the rupture process resulting in a corresponding plastic loss (Figs. (8)-(9)). To make the relationship between the hydrogen induced damages and mechanical characteristic of X80 steel clearly, a comparison between the results in Fig. 4 and Table. 1 is made as shown in Fig. 11. It can be seen that the HIC susceptibility parameters, both $I_\delta$ and $I_\psi$, are mostly in linear relationship to the scale of HIC. It means that HIC plays an important role in determining the mechanical reliability of the as-received X80 steel.

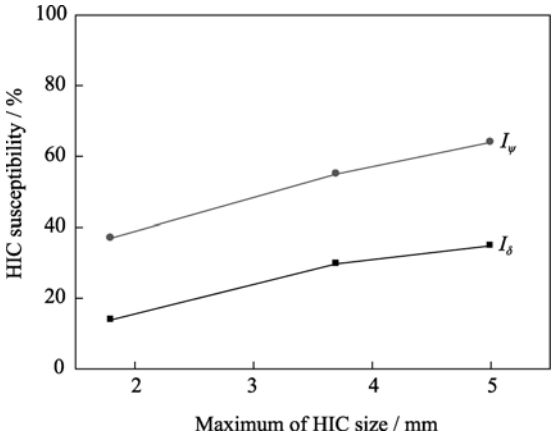


**Fig. 11. HIC susceptibility of X80 steel varied as a function of the maximum of HIC scale after charging in 0.5 mol/L $H_2SO_4$ and $I$=20 mA/cm$^2$.**

## 4. Conclusions

(1) The increase of charging time and charging current density, or the concentration of charging solution leads to an increase of the hydrogen content in X80 steel, which plays a key role in the initiation and propagation of HIC.

(2) The majority of macro-inclusions within the as-used X80 steel do not constitute a direct threat to hydrogen induced cracking except aluminum oxides, which directly or indirectly lead to HIC.

(3) The hydrogen trap density at room temperature of the as-used X80 pipeline steel is estimated to be pretty high, which is an essential reason why the steel is sensitive to HIC. After electrochemical hydrogen charging, the elongation loss rates and area reduction of X80 steel decline obviously, taking a noticeable sign of hydrogen-induced plasticity damages. It is demonstrated that the losses of these plastic parameters have a linear relation to the fracture size due to hydrogen.

## References

[1] W.W. Li, L. Shen, L.S. Han, *et al.*, Welding experiment on X80 pipeline steel, *Hot Work. Technol.*, 35(2006), No.11, p.26.

[2] M. Zhang, C.W. Yao, C. Fu, and Z.L. Lu, Submerged arc welding wire matched with X80 pipeline steel, *Trans. China Weld. Inst.*, 27(2006), No.4, p.64.

[3] P. Liang, C.W. Du, X.G. Li, *et al.*, Effect of hydrogen on the stress corrosion cracking behavior of X80 pipeline steel in Ku'erle soil stimulated solution, *Int. J. Miner. Metall. Mater.,* 16(2009), No.4, p.407.

[4] Y.T. Li, Z. Du, Y.Y. Tao, and L.Y. Xiong, Sulfide stress cracking of X70 pipeline steels, *Trans. China Weld. Inst.*, 24(2003), No.3, p.76.

[5] Z.Y. Liu, G.L. Zhai, X.G. Li, *et al.*, Effect of deteriorated microstructures on SCC of X70 pipeline steel in acid soil environment, *Int. J. Miner. Metall. Mater.,* 15(2008), No.6, p.707.

[6] D. Hardie, E.A. Charles, and A.H. Lopez, Hydrogen embrittlement of high strength pipeline steels, *Corros. Sci.*, 48(2006), No.12, p.4378.

[7] S.Y. Shin, B. Hwang, S. Lee, *et al.*, Correlation of microstructure and charpy impact properties in API X70 and X80 line-pipe steels, *Mater. Sci. Eng. A*, 458(2007), No.1-2, p.281.

[8] A. Shterenlikht, S.H. Hashemi, I.C. Howard, *et al.*, A specimen for studying the resistance to ductile crack propagation in pipes, *Eng. Fract. Mech*., 71(2004), No.13-14, p.1997.

[9] J.H. Kong, L. Zhen, B. Guo, *et al.*, Influence of Mo content on microstructure and mechanical properties of high strength pipeline steel, *Mater. Des.*, 25(2004), No.8, p.723.

[10] C.F. Dong, X.G. Li, Z.Y. Liu, and Y.G. Zhang, Hydrogen-induced cracking and healing behaviour of X70 steel, *J. Alloys Compd.*, 484(2009), No.1-2, p.966.

[11] T. Zhang, W.Y. Chu, K.W. Gao, and L.J. Qiao, Study of correlation between hydrogen-induced stress and hydrogen embrittlement, *Mater. Sci. Eng. A*, 347(2003), No.1-2, p.291.

[12] C. Pan, Y.J. Su, W.Y. Chu, *et al.*, Hydrogen embrittlement of weld metal of austenitic stainless steels, *Corros. Sci.*, 44(2002), No.9, p.1983.

[13] X.C. Ren, W.Y. Chu, J.X. Li, *et al.*, The effects of inclusions and second phase particles on hydrogen-induced blistering in iron, *Mater. Chem. Phys.*, 107(2008), No.2-3, p.231.

[14] Z.Y. Liu, X.G. Li, C.W. Du, *et al.*, Effect of inclusions on initiation of stress corrosion cracks in X70 pipeline steel in an acidic soil environment, *Corros. Sci.*, 51(2009), No.4, p.895.

[15] J.Y. Yoo, J.F. Jiang, and L.L. Zhou, The advantage of spicular ferrite pipeline steel X70—The development of transmitting oil & gas pipeline industry in atrocious weather, *Trans. China Weld. Inst.*, 27(2004), No.2, p.9.

[16] W.Y. Chu, *Hydrogen Damage and Lag Fracture*, Metallurgical Industry Press, Beijing, 1988, p.79.

[17] S.H. Wang, W.C. Luu, K.F. Ho, *et al.*, Hydrogen permeation in a submerged arc weldment of TMCP steel, *Mater. Chem. Phys.*, 77(2003), No.2, p.447.

[18] K. Banerjee and U.K. Chatterjee, Hydrogen permeation and hydrogen content under cathodic charging in HSLA 80 and HSLA 100 steels, *Scripta Mater.*, 44(2001), No.2, p.213.

[19] S.K. Yen and I.B. Huang, Hydrogen permeation tests in laminates: application to grain/grain boundary of AISI430 stainless steel, *Corrosion*, 59(2003), No.11, p.995.